Optical imaging of hard and soft dental tissues using discretely swept optical frequency domain reflectometry optical coherence tomography at wavelengths from 1560 to 1600 nm

Hideo Kakuma
University of Tokyo
Research Center for Advanced Science and
    Technology
4-6-1, Komaba, Meguro-ku
Tokyo 153-8904, Japan

Kohji Ohbayashi
Kitasato University
Center for Natural Science
Sagamihara-si
Kanagawa 228-8555, Japan

Yasuhiko Arakawa
University of Tokyo
Research Center for Advanced Science and
    Technology
4-6-1, Komaba, Meguro-ku
Tokyo 153-8904, Japan

Abstract. We have been developing a Mach-Zehnder type of optical frequency domain reflectometry optical coherence tomography (OFDR-OCT) that uses discretely swept superstructure-grating distributed Bragg- reflector (SSG-DBR) lasers developed for telecommunication fields and has a 12-mm-depth range. We report images obtained with L-band (1560 to 1600 nm) and C-band (1529 to 1568 nm) SSG-DBR sources at 0.5 μs/step, which is 20 times faster than the scanning speed used to obtain the images we reported previously. Despite the faster scanning, we obtain good OCT images of both hard and soft dental tissues *in vitro* and *in vivo*. © *2008 Society of Photo-Optical Instrumentation Engineers.* [DOI: 10.1117/1.2839042]

1 Introduction

Since the first implementation of optical coherence tomography (OCT), it has proven to be a useful medical diagnostic technique.[1] Three OCT methods have been developed so far: time-domain OCT (TD-OCT),[1] spectral-domain OCT (SD-OCT),[2] and optical frequency domain reflectometry OCT (OFDR-OCT).[3] Several groups of investigators have studied of dental tissue by using TD-OCT[4,5] and SD-OCT,[6] and have shown that a depth range greater than 5 mm is needed for *in vivo* diagnosis of multiple teeth simultaneously. For sufficiently deep penetration into dental tissues, high sensitivity is also required. Both SD-OCT and OFDR-OCT are Fourier-domain OCT (FD-OCT), and the sensitivity of FD-OCT has been demonstrated to be 20 to 30 dB better than that of TD-OCT.[7,8] FD-OCT is also faster than TD-OCT. Aberration of the lens in the spectrometer used in the SD-OCT configuration limits the depth range of SD-OCT to less than about 2.5 mm,[9] and greater depth ranges have been obtained by using OFDR-OCT.[10,11] Another reason that OFDR-OCT is better for dentistry is that the SD-OCT configuration, having a spectrometer and a charge-coupled device, is more complex than the OFDR-OCT configuration. We have been developing an OFDR-OCT system, using as a discretely swept source the superstructure-grating distributed Bragg reflector (SSG-DBR) lasers[12–14] originally developed for telecommunications applications. The OCT images of an extracted tooth that we could obtain *in vitro* with that source, at a scanning speed 10 μs per step, had a depth range of 6 mm.[10,15]

In the work presented here, OCT imaging of both hard and soft dental tissues with the system, we have not only extended the depth range to 12 mm by using a SSG-DBR laser with a longer wavelength to reduce scattering by tissues, but have also reduced motion artifacts by increasing the scanning speed to 0.5 μs per step.

2 Theory

Figure 1 shows the fiber optic Mach-Zehnder interferometer configuration of the OFDR-OCT system with a SSG-DBR laser as the light source. The principles and theory of the system have already been reported,[3,10] so we describe them only briefly. The light from the source is split into the sample and reference arms by coupler 1. In the sample arm, light illuminates the sample and the light reflected from the sample is received. In the reference arm, light is reflected by the reference mirror. Both lights are combined by coupler 2, which outputs the interference signal. It is detected by the balanced photoreceiver.

The SSG-DBR laser emits light at N discrete wavenumbers $k_i = k_0 + i\delta k_i, (i = 1, 2 \ldots N)$. The photoreceiver current $I_{d,i}$ at the wave number k_i is described as

Address all correspondence to Hideo Kakuma, R&D, The Yoshida Dental Mfg. Co., Ltd., 1–3–6 Kotobashi Sumidaku, Tokyo 130–8516, Japan; Tel: +81–3–3631–2165; Fax: +81–3–3635–6910; E-mail: kakuma@yoshida-net.co.jp
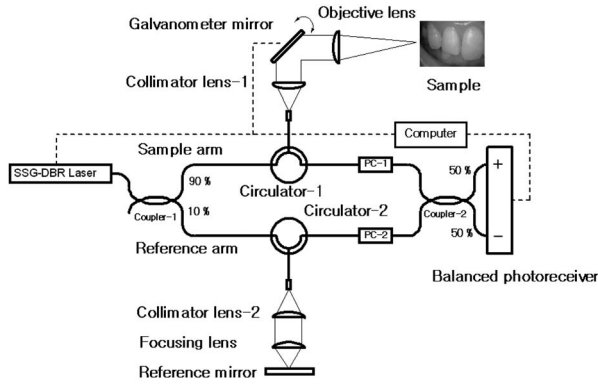
Fig. 1 Experimental setup of the OFDR-OCT system.

$$I_{d,i} = \frac{\eta q}{h\nu}\left\{ p_r + p_0 \int r^2(z)dz \right.$$

$$\left. \pm 2\sqrt{p_r p_0} \int r(z)\Gamma(z)\cos[2k_i z + \phi(z)]dz \right\}, \quad (1)$$

where η is the photoreceiver sensitivity, q is the quantum electric charge, $h\nu$ is the single-photon energy, p is the power reflected from the reference arm, p_0 is the optical power illuminating the sample, z is the axial coordinate corresponding to the optical path length difference, $\phi(z)$ is the phase, and $\Gamma(z)$ is the coherence function. The first and second terms are related to the DC background and the third term is the interferometric signal. Now we consider the simple setting in which a single reflector with reflectivity r^2 is located at $z = z_0$ and the reflectivity profile is given by a delta function: $r(z) = r\delta(z - z_0)$. Since the laser has a long coherence length, we can set $\Gamma(z) = 1$ and obtain

$$I_{d,i} = \frac{\eta q}{h\nu}\left\{ 2\sqrt{p_r p_0} \int r\delta(z - z_0)\cos[2k_i z]dz \right\}$$

$$= \frac{\eta q}{h\nu}2\sqrt{p_r p_0}\, r\cos(2k_i z_0) = \frac{\eta q}{h\nu}2\sqrt{p_r p_s}\cos(2k_i z_0), \quad (2)$$

where $r^2 = p_s/p_0$ and we can consider $\phi(z)$ a factor that can be disregarded. Abrupt changes of the phase owing to mode hopping of the laser source do not affect the data. To get an axial profile of the reflectivity as a function of z, we use discrete Fourier transforms of the interference signal current:
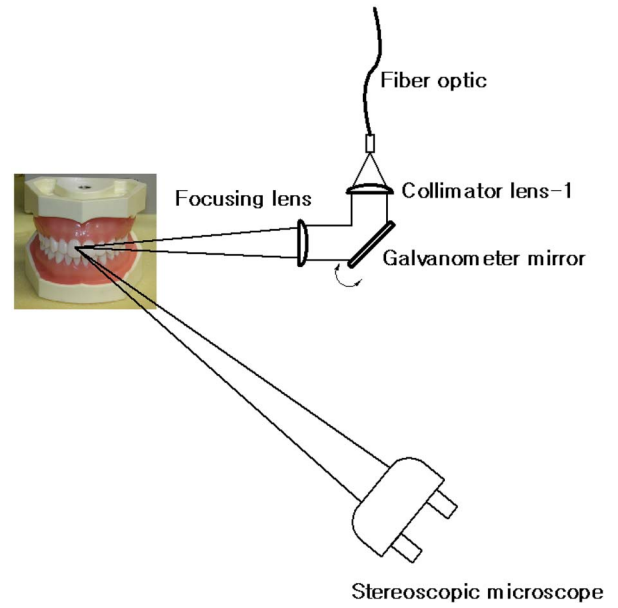
Fig. 2 Setup for *in vitro* imaging.

$$F_c(z) = \frac{\eta q}{h\nu}2\sqrt{p_r p_s}\sum_{i=1}^{N}\cos(2k_i z_0)\cos(2k_i z), \quad (3)$$

$$Fs(z) = \frac{\eta q}{h\nu}2\sqrt{p_r p_s}\sum_{i=1}^{N}\cos(2k_i z_0)\sin(2k_i z). \quad (4)$$

The axial profile of reflectivity r^2 is proportional to the following function:

$$F_t(z)^2 = F_c(z)^2 + F_s(z)^2, \quad (5)$$

where $F_t(z)^2$ can be calculated by

$$F_t(z)^2 = r^2\left(\frac{\eta q}{h\nu}\right)^2 p_r p_0\left(\left\{\frac{\sin[\Delta k(z - z_0)]}{\sin[\delta k(z - z_0)]}\right\}^2 \right.$$

$$\left. + \left\{\frac{\sin[\Delta k(z + z_0)]}{\sin[\delta k(z + z_0)]}\right\}^2 + B(z)\right), \quad (6)$$

in which function $B(z)$ is

Table 1 Specification of the SSG-DBR lasers.

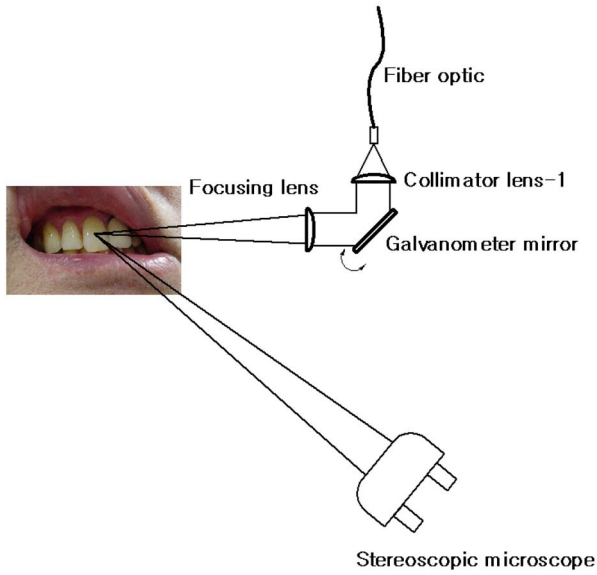|	Wavelength λ (nm)	Tunable range (nm)	Frequency interval $\delta\nu$ (GHz)	Wavenumber interval δk(cm^{-1})	Scanning speed (μs)	A-line rate (kHz)
C-band	1529.46 to 1567.86	38.40	6.25	1.31	10 or 0.5	0.13 or 2.6
L-band	1559.99 to 1599.96	39.97	6.25	1.31	0.5	2.6

Fig. 3 Setup for *in vivo* imaging.

$$B(z) = 2 \cos\{[4k_0 + 2(N+1)\delta k]z_0\}$$
$$\times \frac{\sin[\Delta k(z - z_0)]}{\sin[\delta k(z - z_0)]} \frac{\sin[\Delta k(z + z_0)]}{\sin[\delta k(z + z_0)]}. \tag{7}$$

From Eq. (6) we obtain the following depth range:[10]

$$\Delta z = \pi/2\delta k. \tag{8}$$

For $\delta k = 2.62 \text{ cm}^{-1}$ and $\delta k = 1.31 \text{ cm}^{-1}$, the depth ranges are respectively 6 and 12 mm. The full width at half maximum (FWHM) of the peaks in Eq. (6) defines the resolution of the axial distance measurement. By numerical calculation, we can obtain the axial resolution[10] δz (FWHM) as

$$\delta z = 2.78/\Delta k, \tag{9}$$

for $\Delta k = N\delta k$, $N = 769$, and $\delta k = 1.31 \text{ cm}^{-1}$, the resolution δz will be 28 μm in air. In a tissue with a refractive index of n, the resolution increases by a factor of $1/n$.

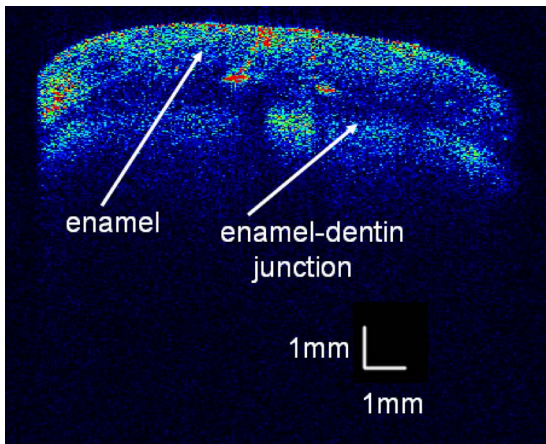**Fig. 4** Image obtained with the C-band source at a scanning speed of 10 μs/step.

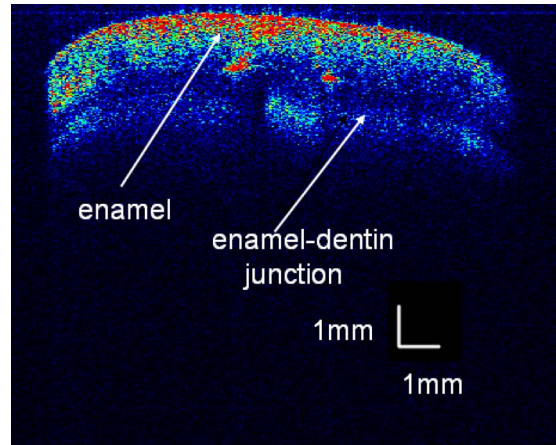**Fig. 5** Image obtained with the C-band source at a scanning speed of 0.5 μs/step.

3 Experimental Setup

The experimental setup is shown in Fig. 1. In this research we used two different SSG-DBR lasers: a C-band laser (wavelength $\lambda = 1529$ to 1568 nm) and an L-band laser ($\lambda = 1560$ to 1600 nm). Our newly developed L-band laser emits light at approximately 0.05-nm wavelength steps. In frequency val-
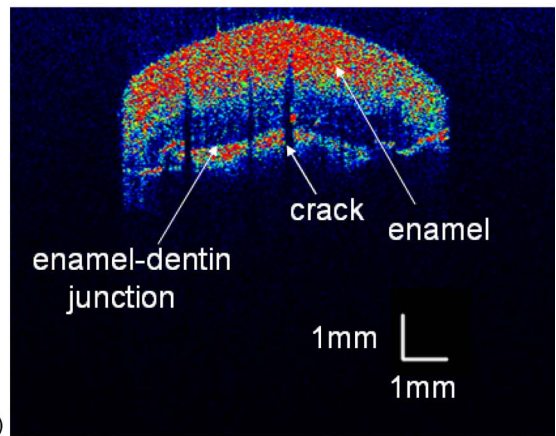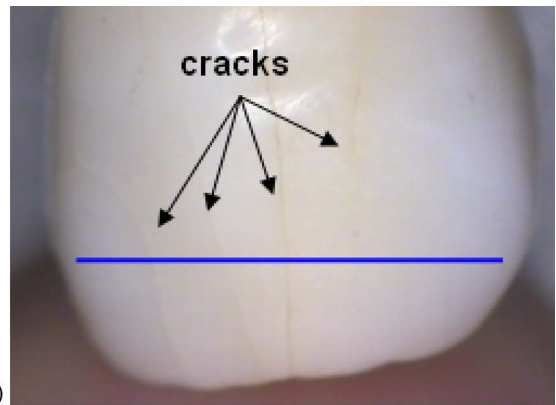

(a)

(b)

Fig. 6 (a) Image of an extracted upper canine. (b) OCT image of the canine.
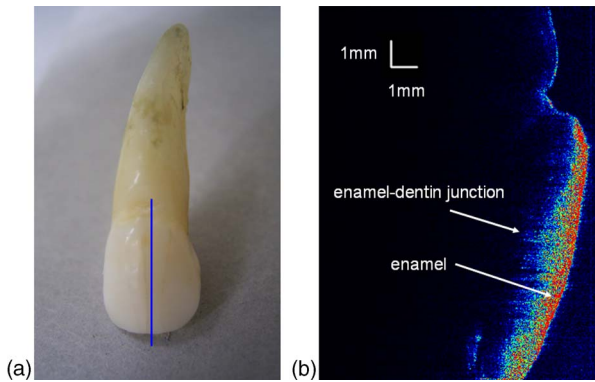
Fig. 7 (a) Whole image of the canine. (b) OCT image of the canine.

ues, the sweep range is from 187 to 192 THz with steps of 6.25 GHz, corresponding to a wavenumber interval of 1.31 cm^{-1}.

The total number N of wavelengths emitted by the source is 769. At the 500-ns/step wavelength scanning speed used in this experiment, the A-scan time is 0.3845 ms. This corresponds to a 2.6-kHz A-line rate. The C-band source we used in our previous works scanned at 10 μs per step.[10,15] The C-band source used in the work reported here was able to scan at 500 ns per step. The specifications of the newly developed C-band and L-band lasers are listed in Table 1.

The light was split into the sample arm and reference arm at the first coupler (coupler 1) with a splitting ratio of 90:10. Light in the sample arm was fed to the input port of circulator 1. Light out of the output/input port of circulator 1 illuminated the sample via the collimator lens, galvanometer mirror, and objective lens with a focal length of 60 mm. Back-reflected light (including back-scattered light) from the sample was gathered with the illuminating optics. Output light from the output port of circulator 1 was fed to coupler 2, with the splitting ratio being 50:50. Light that passed through the reference arm was also fed to coupler 2, from which the interference signal was obtained. Polarization controllers PC 1 and PC 2 adjusted the polarization dispersion in both arms to maximize the interference signal.

Figures 2 and 3 show the setups for *in vitro* and *in vivo* imaging. We did not use a special dentistry probe but instead used a commercially available OCT probe for the anterior segment of the eye. The targeted teeth could be seen with the stereoscopic microscope. For *in vivo* imaging (Fig. 3), we rested the head on a chin rest of the probe and lifted the upper lip to expose the teeth. In this situation, we could not access molars or premolars because the lips were in the way. In the *in vitro* imaging, however, we could access the phantom at any angle and view multiple teeth.

4 Results and Discussion

Images of an extracted lower lateral incisor that were obtained with the C-band source at scanning speeds of 10 and 0.5 μs per step are shown in Figs. 4 and 5. Comparing the obtained two OCT images, one sees that the 20-fold increase in scanning speed did not cause any deterioration of the image quality. In air, the estimated depth range and resolution were respectively 12 mm and 28 μm. As seen in those figures, the
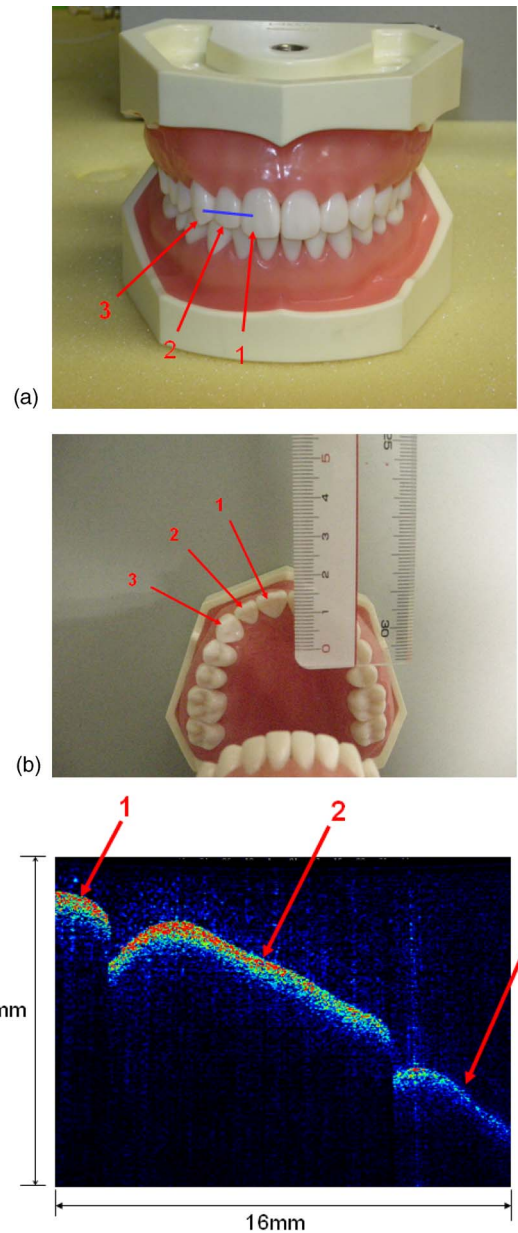

Fig. 8 (a) Phantom seen from front. (b) Phantom seen from bottom. (c) OCT image of three phantom teeth.

depth of the images extends over an optical length greater than 5 mm, which indicates need for an imaging depth range greater than 5 mm.

Images of an extracted upper canine that were obtained with the L-band source are shown in Figs. 6 and 7. Because we found no difference of OCT image quality between the L-band source and with the C-band source, we carried out all the following OCT imaging with the L-band source. The blue lines in the photographs in Figs. 6(a), 7(a), and 8(a) indicate the scanning direction.

To verify the capability of obtaining 12-mm OCT images, we imaged the teeth of a phantom. Figure 8(a) shows a picture in which three teeth of the phantom are numbered 1, 2, and 3. The scale in Fig. 8(b) is an aid to indicate the physical length of the gather of the three teeth. As the scale shows, the length
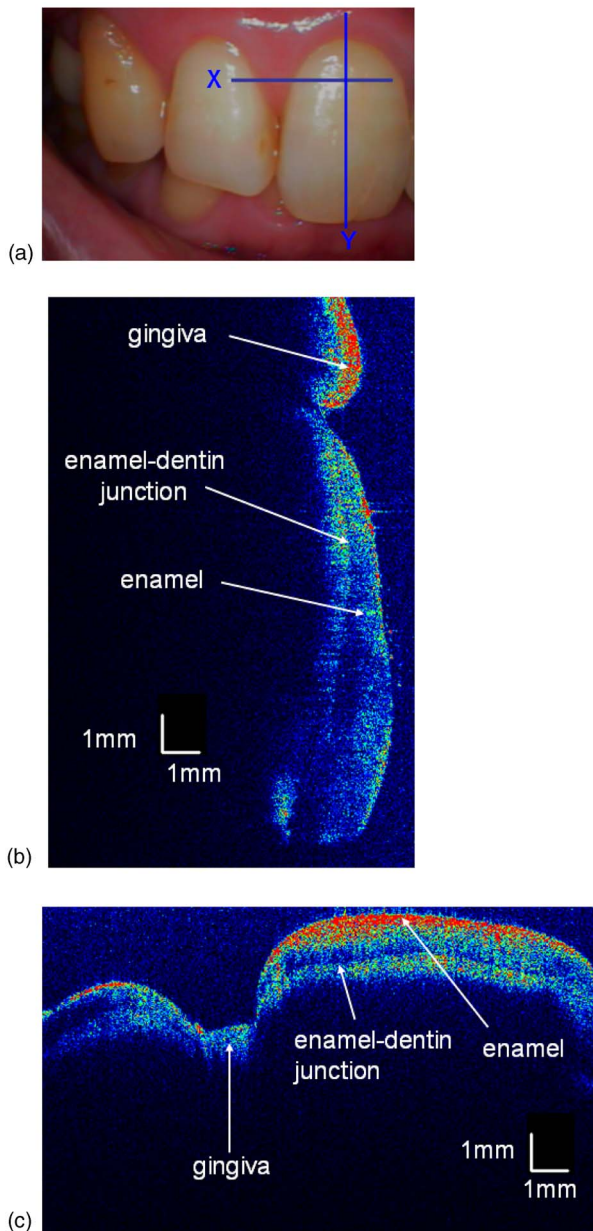
Fig. 9 (a) Image of target teeth, showing scanning directions X and Y. (b) OCT image (line X) of the tooth shown in (a). (c) OCT image (line Y) of the tooth shown in (a).

is about 12 mm. The result of OCT imaging of the three teeth is shown in Fig. 8(c). The vertical length of the OCT image is 12 mm, verifying the capability of imaging a 12-mm-depth range.

We extended our work to *in vivo* imaging of teeth, and Fig. 9(a) is a photograph of the target teeth. The lines labeled X and Y are the horizontal and vertical directions in which OCT imaging was performed, and Figs. 9(b) and 9(c) are OCT images obtained in those directions. The enamel-dentin junction is clearly seen all over the OCT images. Soft and hard tissues (gingiva, enamel, and dentin) are distinguished clearly, but the image of the hard tissue under the soft tissue was indistinct. Unfortunately, because of the lip barrier and the restrictions due to using an OCT probe designed for the ante-

rior segment of the eye, we did not have access to the occlusal pits and fissures areas in which most dental caries are found. We therefore need to develop a specifically designed dental probe.

5 Conclusion

We perform *in vitro* OCT imaging of an extracted canine by using a newly developed C-band SSG-DBR source, and find that the image quality obtained at a scanning speed of 0.5 μs/step does not differ from that obtained at 10 μs/step. Our newly developed SSG-DBR sources enable scanning at a wavenumber step of 1.31 cm^{-1}, corresponding to a 12-mm-depth range. This depth range was confirmed by obtaining OCT images of a tooth phantom. We can clearly see the enamel-dentin junction in *in vitro* OCT images of an extracted canine that are obtained with the newly developed L-band SSG-DBR source. We can also see the enamel-dentine junction in OCT images obtained *in vivo*. This OCT system can be used for early detection of dental caries if we develop a dental probe providing access to occlusal pits and fissures.

References

1. D. Huang, E. A. Swanson, C. P. Lin, J. S. Schuman, W. G. Stinson, W. Chang, M. R. Hee, T. Flotte, K. Gregory, C. A. Puliafito, and J. G. Fujimoto, "Optical coherence tomography," *Science* **254**, 1178–1181 (1991).
2. J. F. de Boer, B. Cense, B. H. Park, M. C. Pierce, G. J. Tearney, and B. E. Bouma, "Improved signal-to-noise ratio in spectral-domain compared with time-domain optical coherence tomography," *Opt. Lett.* **28**, 2067–2069 (2003).
3. S. H. Yun, G. J. Tearney, J. F. de Boer, N. Iftimia, and B. E. Bouma, "High-speed optical frequency-domain imaging," *Opt. Express* **11**, 2953–2963 (2003).
4. B. Colston, U. Sathyam, L. DaSilva, M. Everett, P. Stroeve, and L. Otis, "Dental OCT," *Opt. Express* **3**, 230–238 (1998).
5. A. Feldchtein, V. Gelikonov, R. Iksanov, G. Gelikonov, R. Kuranov, A. Sergeev, N. Gladkova, M. Ourutina, D. Reitze, and J. Warren, "In vivo OCT imaging of hard and soft tissue of the oral cavity," *Opt. Express* **3**, 239–250 (1998).
6. V. Dimitrova Madjarova, Y. Yasuno, S. Makita, Y. Hori, J. B. Voeffray, M. Itoh, T. Yatagai, M. Tamura, and T. Nanbu, "Investigations of soft and hard tissues inoral cavity by spectral domain optical coherence tomography," *Proc. SPIE* **6079**, 60790N (2006).
7. M. Choma, M. Sarunic, C. Yang, and J. Izatt, "Sensitivity advantage of swept source and Fourier domain optical coherence tomography," *Opt. Express* **11**, 2183–2189 (2003).
8. R. Leitgeb, C. K. Hitzenberger, and A. F. Fercher, "Performance of Fourier domain vs. time domain optical coherence tomography," *Opt. Express* **11**, 889–894 (2003).
9. S. H. Yun, G. J. Tearney, B. E. Bouma, B. H. Park, and J. F. de Boer, "High-speed spectral domain optical coherence tomography at 1.3 μm wavelength," *Opt. Express* **11**, 3598–3604 (2003).
10. T. Amano, H. Hiro-Oka, D. Choi, H. Furukawa, F. Kano, M. Takeda, M. Nakanishi, K. Shimizu, and K. Ohbayashi, "Optical frequency-domain reflectometry with a rapid wavelength-scanning superstructure-grating distributed Bragg reflector laser," *Appl. Opt.* **44**, 808–816 (2005).
11. R. Huber, K. Tairn, M. Wojtkowski, and I. G. Fujimoto, "Fourier domain modde locked lasers for swept source OCT imaging at up to 290 kHz scan rates," *Proc. SPIE* **6079**, 60790U-1 (2006).

12. Y. Tohmori, Y. Yoshikuni, H. Ishii, F. Kano, T. Tamamura, Y. Kondo, and M. Yamamoto, "Broad-range wavelength-tunable superstructure grating (SSG) DBR lasers," *IEEE J. Quantum Electron.* **29**, 1817–1823 (1993).
13. H. Ishii, H. Tanobe, F. Kano, Y. Tohmori, Y. Kondo, and Y. Yoshikuni, "Quasicontinuous wavelength tuning in super-structure-grating (SSG) DBR lasers," *IEEE J. Quantum Electron.* **32**, 433–441 (1996).
14. H. Ishii, F. Kano, Y. Yoshikuni, and H. Yasaka, "Mode stabilization method for superstructure-grating DBR lasers," *J. Lightwave Technol.*, **16**, 433–442 (1998).
15. T. Amano, H. Hiro-Oka, D. Choi, H. Furukawa, F. Kano, M. Takeda, M. Nakanishi, K. Shimizu, and K. Ohbayashi, "OFDR with an SSG-DBR laser," *Proc. SPIE* **5531**, 5531-47 (2004).